

**RESEARCH ARTICLE**

# Dihydrogen phosphate anion boosts the detection of sugars in electrospray ionization mass spectrometry: A combined experimental and computational investigation

Alexander Ruf<sup>1,2,3</sup> | Basem Kanawati<sup>1</sup>  | Philippe Schmitt-Kopplin<sup>1,2</sup>

<sup>1</sup>Analytical BioGeoChemistry, Helmholtz Zentrum München, Munich, Germany

<sup>2</sup>Analytical Food Chemistry, Technische Universität München, Munich, Germany

<sup>3</sup>Université Aix-Marseille, Laboratoire de Physique des Interactions Ioniques et Moléculaires (PIIM), Marseille, France

**Correspondence**

A. Ruf and B. Kanawati, Analytical BioGeoChemistry, Helmholtz Zentrum München, Munich, Germany.

Email: rufalexan@gmail.com; basem.kanawati@helmholtz-muenchen.de

**Funding information**

Helmholtz Zentrum München

**Rationale:** Sugars are key molecules of life but challenging to detect via electrospray ionization mass spectrometry (ESI-MS). Unfortunately, sugars are challenging analytes for mass spectrometric methods due to their high gas-phase deprotonation energies and low gas-phase proton affinities which make them difficult to ionize in high abundance for MS detection.

**Methods:** Hydrogen-bond interactions in  $\text{H}_2\text{PO}_4^-$ -saccharide anionic systems were studied both experimentally (via electrospray ionization Fourier transform ion cyclotron resonance mass spectrometry, ESI-FT-ICR-MS) and computationally by several sophisticated density-functional theoretical methods (DFT and DFT-D3).

**Results:** The  $\text{H}_2\text{PO}_4^-$  dopant boosts the detection of sugars up to 51-times in the case of sucrose and up to 263-times for glucose (at 0.1 ppm concentration level).  $\text{H}_2\text{PO}_4^-$  binds toward sugar molecules with noticeably more hydrogen bonds than the established dopant chloride  $\text{Cl}^-$  does, with increasing binding energies in the order: Monosaccharides < Trisaccharides < Disaccharides. Analysis of a complex oak plant sample revealed that  $\text{NH}_4\text{H}_2\text{PO}_4$  specifically labeled a diverse set of sugar-type plant metabolites in the form of  $[\text{M} + \text{H}_2\text{PO}_4]^-$  complexes.

**Conclusions:** We reveal the mechanism of interaction of  $\text{H}_2\text{PO}_4^-$  with different sugars and glycosylated organic compounds, which significantly enhances their ionization in mass spectrometry. A computational and experimental investigation is presented. A strong correlation between the MS signal intensities of detected  $[\text{M} + \text{H}_2\text{PO}_4]^-$  anions of different saccharides and their calculated dissociation enthalpies was revealed. Thus, the variation in MS signal intensities can be very well described to a large extent by the variation in calculated saccharide affinities toward the  $\text{H}_2\text{PO}_4^-$  dopant anion, showing that DFT-D3 can very well describe experimental FT-ICR-MS observations.

This is an open access article under the terms of the Creative Commons Attribution-NonCommercial-NoDerivs License, which permits use and distribution in any medium, provided the original work is properly cited, the use is non-commercial and no modifications or adaptations are made.

© 2022 The Authors. *Rapid Communications in Mass Spectrometry* published by John Wiley & Sons Ltd.

## 1 | INTRODUCTION

Sugars represent a key class of organic compounds among all living systems as they are the building blocks of nucleic acids DNA and RNA.<sup>1</sup> This makes them one of the most attractive analytical targets, for instance in prebiotic chemistry and origins of life research.<sup>2,3</sup> Unfortunately, sugars are challenging analytes for mass spectrometric methods but also in general due to their high structural complexity.<sup>4</sup> From a thermodynamic point of view, sugars possess high gas-phase deprotonation energies and low gas-phase proton affinities which makes them difficult to ionize and thus to be observed via electrospray ionization mass spectrometry (ESI-MS).<sup>5</sup> As a result, sugars are characterized by low ionization efficiencies and thus by low ion signal intensities in mass spectrometry. Sugars (mono-, di- and trisaccharides) have been widely used as model analytes for screening anionic dopants in negative mode electrospray ionization mass spectrometry [(-)ESI-MS].<sup>6,7</sup>

Dopants represent powerful agents in ESI-MS for enabling the detection of organic molecules, which cannot be easily ionized.<sup>8–11</sup> As a result of non-covalent interactions between charged dopant additives and neutral substrate molecules, analytes can be ionized. This strategy was successfully discerned by several research groups in the past, elucidating the interaction of neutral substrates with both positive<sup>10,12–14</sup> and negative ions in ESI-MS.<sup>6–9,11</sup> Previous work from matrix-assisted laser/desorption ionization (MALDI)-MS experiments, performed on various biological proteins, revealed that endogenous phosphate salts give rise to high signal intensities of phosphate-adduct ions of large molecular weight N-linked glycans, derived from several biological sources.<sup>15–17</sup> However, our current study presents the first investigation, performed on a very low molecular metabolic scale, which examines mono-, di-, and trisaccharides as low level molecular backbones for low-mass molecules for metabolomic studies. Moreover, we show for the first time that the  $\text{H}_2\text{PO}_4^-$  dopant ion efficiency can even be thoroughly examined by high-level theoretical DFT-D3 calculations, delivering excellent agreement between the experimental and theoretical findings.

Chloride ( $\text{Cl}^-$ ) represents a popular dopant which is often used to solve the ionization problem of sugars in ESI-MS.<sup>7,9</sup>  $\text{Cl}^-$  dopants are good candidates for the formation of stable sugar- $\text{Cl}^-$  complexes with saccharide molecules. It efficiently forms hydrogen bonds toward neutral OH-bearing molecules due to the high electronegativity of the dopant's center. Understanding the mechanism of interaction of the chloride anion with a neutral sugar molecule is of high importance because it enables the estimation of the analyte's binding affinity toward the charged dopant. Boutegrabet et al achieved excellent agreement between computed and experimentally deduced binding affinities between chloride anions and several sugar molecules.<sup>7</sup> The coordination number has been found to be a major parameter in influencing sugar-chloride binding affinities. Sucrose was shown to bind stronger toward chloride, than glucose or melezitose does.<sup>7</sup> New ideas for investigating anionic dopants have been steadily ongoing to enhance ionization efficiencies and, thus, decrease the limit of detection. As a second aim is specificity of detection by

$[\text{M} + \text{dopant}]^-$  complexes, enhancing selectivity in comprehensive analyses of complex mixtures. The aim of this work is to further improve the ionization efficiency for sugars, compared with the established chloride dopants. Second, excellent agreement between experimental and theoretical findings was obtained. Third, the novel dopant should be applied to real samples bearing sugar-type plant metabolites (glycosides). Thus, the strategy of this study is driven by both targeted and non-targeted analysis.

$\text{H}_2\text{PO}_4^-$  represents an electron-delocalized tetrahedral which possesses multiple interaction sites to form more than one non-covalent bond (e.g. via hydrogen bonds) toward neutral target molecules.<sup>15</sup> Furthermore, there is evidence that  $\text{H}_2\text{PO}_4^-$  forms strong hydrogen bonds.<sup>16,17</sup> Electron delocalization between one double-bonded oxygen atom, two hydroxy groups and a negatively charged oxygen atom results in twelve canonical forms to be written for the dihydrogen phosphate anion and arguing for its high stability. This mesomeric effect leads to an overall homogeneous electron density distribution between different functional groups.  $\text{Cl}^-$  is a spherical one atomic system and has a limited effective surface when compared with multi-atomic dopants and this fact increases the potential of  $\text{H}_2\text{PO}_4^-$  as a powerful dopant.

## 2 | EXPERIMENTAL

### 2.1 | Sample preparation

Sugars (glucose, galactose, sucrose, gentiobiose, melezitose) and ammonium dihydrogen phosphate and ammonium chloride (of analytical grade; purity >98%) were purchased from Sigma-Aldrich (Steinheim, Germany). Raffinose (analytical grade; purity >98%) was obtained from Fluka. For the plant metabolites, quercetin and kaempferol were purchased from Roth (Karlsruhe, Germany) and their monoglucosylated organic compounds from Extrasynthese (Genay Cedex, France). Salicyl alcohol and salicin were purchased from Sigma-Aldrich (also in analytical grade). All solvents used (methanol, water, acetonitrile) were of chromatographic grade.

Stock solutions of the sugars, aglycones and glycoside analytes were prepared by dissolving each substance in water at a concentration of 1,000 mg/mL. Two sugar mixtures containing a mono- (glucose and galactose), di- (sucrose and gentiobiose), and trisaccharide (melezitose and raffinose) were prepared. The concentrations of those two mixture solutions were 1 ppm, accordingly, except of those experiments denoted by a sugar concentration of 0.1 ppm.

Solutions of the studied dopants were prepared, starting from a stock solution containing 10 mM of the dopant. Experiments with a sugar concentration of 0.1 ppm were performed with a dopant starting concentration of 1 mM of the dopant. The dilutions were done in water. From anionic stock solutions, volumes of 5  $\mu\text{L}$  up to 50  $\mu\text{L}$  in 5  $\mu\text{L}$  steps were added to 1000  $\mu\text{L}$  of the sugar mixture.

Plant extracts for the non-targeted analysis of the complex oak plant sample were prepared using the following procedure. All steps

were performed below 5°C to avoid metabolic activity, due to the presence of proteins. In a first step, the plant sample (oak *Quercus robur* from North-Rhine-Westphalia<sup>18</sup>) was ground with a pestle and homogenized. Subsequently, the weight of the sample was determined ( $\approx 40$  mg) in liquid nitrogen and 2000  $\mu\text{L}$  of a methanol/ $\text{H}_2\text{O}$  mixture (7/3, v/v) was added to the sample. Next, metabolites were extracted for 15 min in an ice-cold ultrasonic bath and centrifuged afterwards for 10 min at 14,000 rpm. Then 800  $\mu\text{L}$  supernatant was mixed with 2000  $\mu\text{L}$  of methanol/ $\text{H}_2\text{O}$  (7/3, v/v) to form the plant stock solution. Five solutions with different dopant concentrations were measured (dopant concentrations of 0  $\mu\text{M}$ , 25  $\mu\text{M}$ , 50  $\mu\text{M}$ , 100  $\mu\text{M}$ , 200  $\mu\text{M}$   $\rightarrow$  solution 00, solution 01, solution 02, solution 03, solution 04), using triplicates for each concentration, added to the plant stock solution. Each sample was diluted 1/20 in  $\mu\text{L}$  of acetonitrile/ $\text{H}_2\text{O}$  (1/1, v/v) for analysis by Fourier transform ion cyclotron resonance mass spectrometry (FTICR-MS).

## 2.2 | FT-ICR-MS experiments

The experimental study was performed on a FT-ICR mass spectrometer from Bruker Daltonics (Bremen, Germany) with a 12 T magnet from Magnex, UK. The spectra for the non-targeted plant extract analysis were acquired with a time-domain transient of 4 MWords. The frequency domain is afterwards converted by the Apex Control program (Bruker Daltonics) into a mass spectrum. Ion excitation was generated in broadband mode (frequency sweep radial ion excitation) and 300 scans were accumulated for each mass spectrum in a mass range of 122–1000 amu (atomic mass units). Ions were accumulated in the hexapole for 300 ms prior to ICR ion detection. The pressure in the ICR vacuum chamber was  $6 \times 10^{10}$  mbar and that in the quadrupole and hexapole regions  $3 \times 10^6$  mbar.

The ESI source (Apollo II, Bruker Daltonics) was used in negative ionization mode to ionize the studied analytes in acetonitrile/water (v/v) solution. The sample solutions were injected directly into the ionization source by means of a  $\mu\text{L}$  pump at a flow rate of 120  $\mu\text{L}/\text{h}$  and were measured as technical triplicates. Due to the fluctuating ionization behavior within the ESI source, the triplicates were treated within an error handling to state the standard deviation, additionally. A source heater temperature of 200°C was maintained and no nozzle-skimmer fragmentation was performed in the ionization source. The instrument was previously calibrated by using arginine negative cluster ions starting from an arginine solution in methanol of 5 mg/L.

(–)ESI-FT-ICR-MS experiments were systematically performed for two sugar mixtures, each containing a mono-, di- and trisaccharide (mixture 1 = {glucose, sucrose, melezitose}, mixture 2 = {galactose, gentiobiose, raffinose}). Each investigated sugar represents a mixture of both  $\alpha$ - and  $\beta$ -stereoisomers. While sugar concentrations were kept constant (1 ppm for each sugar), we varied  $\text{NH}_4\text{H}_2\text{PO}_4$  dopant concentrations from 0 to 500  $\mu\text{M}$  to experimentally test  $[\text{M} + \text{H}_2\text{PO}_4]^-$  reaction characteristics.  $\text{NH}_4\text{Cl}$  was used as a reference dopant in all experiments.

## 2.3 | DFT computations

The electronic structure calculations were performed on a stand-alone computer by density functional theory (DFT) as implemented in Gaussian 09.<sup>19</sup> The hybrid DFT functional B3LYP was implemented with 1d polarization functions for each heavy atom and 1p for each hydrogen atom B3LYP/6-31+G(d,p) in all geometry optimizations and frequency calculations of the optimized geometries. For single point energy calculations, 2d polarization functions for each heavy atom and 1p for each hydrogen atom were used B3LYP/6-311+G(2d,p). The use of diffuse functions also in the geometry optimization runs was very important to correctly describe the structures and energies of the investigated anions.

For geometry optimization, the Bery analytical gradient optimization routines<sup>20,21</sup> were used. The requested convergence in the RMS density matrix was  $1 \times 10^{-8}$ , the threshold value for maximum displacement was 0.0018 and that for the maximum force was 0.00045 Hartree/Bohr. Stationary points were identified by calculating and diagonalizing the Hessian matrix (force constant matrix). All geometries of electronic structures calculated were visualized with the GaussView program.<sup>22</sup>

Frequency calculations were also carried out for each optimized geometry with the same 6-31+G(d,p) basis set to obtain the zero-point vibrational energy (ZPVE). This value was multiplied by a scaling factor of 0.9804 to correct for vibrational anharmonicities, because the DFT methods originally assume harmonic vibrational oscillator, when calculating the vibrational frequencies of oscillating atoms in molecules.<sup>23</sup> Another reason for performing the frequency analysis is to check that the obtained optimized geometry does not represent a transition state or any other higher order saddle point. Single-point energy (SPE) calculations were done at the 6-311+G(2d,p) level of theory.

Dispersion-corrected DFT-D3 geometry optimization calculations were performed by the use of the M06-2X functional and Def2TZVP basis set, starting from the optimized geometries, obtained previously at the B3LYP/6-31+(d,p) level of theory. After the new DFT-D3 optimized geometries of the  $[\text{M} + \text{D}]^-$  complex anions had been obtained, single-point energy calculations were performed on them based on the M06-2X/Def2TZVP level of theory. Stability tests were also performed on all the optimized geometries to ensure that the used wave function represents the lowest energy solution of the self-consistent field (SCF) equations. All molecular systems were treated as restricted shell electronic systems.

The total energy of each molecular system was computed as sum of thermal (enthalpy H at 298 K) and electronic free energies, corrected by a scaled zero-point vibrational energy, ZPVE, expressed as zero-point corrections (ZPC) of respective substrate and dopant species.

$$E = H(298\text{K}) - \text{ZPC} + \text{ZPC} * f(\text{anharmonicities}) + \text{SPE}.$$

The binding energy (BE) between each studied neutral substrate molecule and the anionic dopant in the gas phase was calculated by the following equation:

$$BE = E(\text{Complex}) - [E(\text{Substrate}) + E(\text{Dopant})]$$

Affinity of a substrate toward a dopant =  $-BE$ .

The dissociation energy (DE) for the complex  $[M + D]^-$  represents the energy required to decompose the complex to  $M + D^-$  and is given by:

$$DE = [E(\text{Substrate}) + E(\text{Dopant})] - E(\text{Complex})$$

DFT computations were applied to the gas phase. Boutegrabet et al.<sup>7</sup> were able to show that non-covalent interactions of anionic-dopant-substrate systems do not heavily depend on the medium of the reaction (whether in the liquid or gas phase). The absolute affinities are different for different media (liquid or gaseous state) but the relative affinities are similar within the range of errors. Thus, all computations were performed in the gas phase.

## 2.4 | Raw data handling (DataAnalysis, Bruker Daltonics)

In the first step, using the program "DataAnalysis", raw data were exported with a signal-to-noise ratio (S/N) = 5. FT-MS artifacts were removed via a power-function resolution filter (signal wiggles) using an in-house software.<sup>24</sup> Inorganic features were removed by a mass defect filter. FT-ICR mass spectra (raw data) were internally recalibrated linearly using fatty acids (standard deviation was approximately 0.2 ppm using 16  $m/z$  ratios, each having an error of <1 ppm). From here on, separate analyses were performed for each dopant ion,  $H_2PO_4^-$  and  $Cl^-$ , respectively. For simplification, we generally name it "Dopant" in the following.

## 2.5 | In silico dopant search (Matlab)

In a second step, a Matlab program was developed by B. Kanawati. Using the developed Matlab code, it was assumed that at the lowest concentration (0 mM anionic dopant concentration: =

solution 00) all found intensities corresponding to  $[M - H]^-$  ions while at the highest concentration (200 mM dopant concentration: = solution 04) the intensities are related to  $[M + \text{dopant}]^-$  adducts. Thus,  $m/z$  values of *in silico*  $[M + \text{Dopant}]^-$  ions have been calculated, via

$$m/z(\text{theoretical}) = m/z(\text{experimental}) + M(H+) + M(\text{Dopant anion})$$

where  $M$  = molar mass. Within the first Matlab program the  $m/z$  ratios, relating to  $[M + \text{Dopant}]^-$  ions (experimental out of solution 04 and theoretical ones out of solution 00), were compared within an error window of 1 ppm.

## 2.6 | Calculation of enrichment factor R (LibreOffice)

The two corresponding intensities, out of solutions 00 and 04, of each merged  $m/z$  ratio were used to calculate the ratio  $R$  as follows:

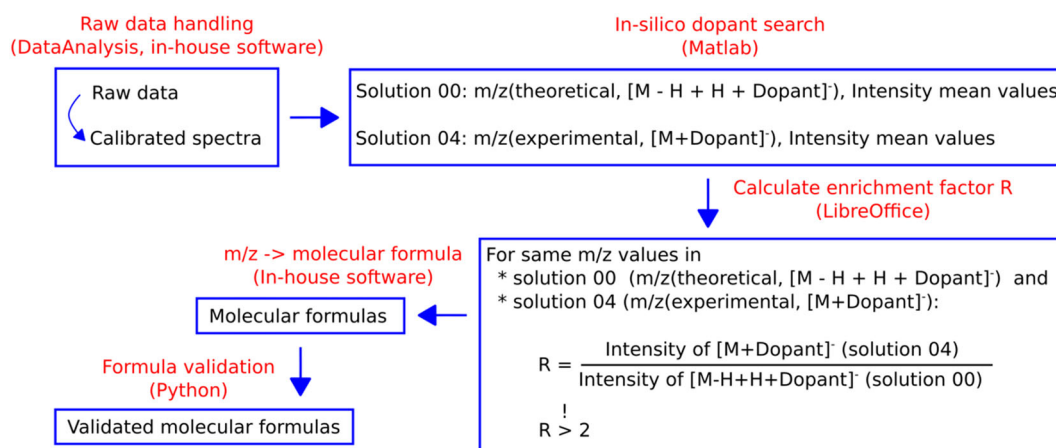
$$R = \frac{\text{Intensity of } [M + D]^- \text{ (solution 04)}}{\text{Intensity of } [M - H + H + D]^- \text{ (solution 00)}}$$

where  $D$  is the  $H_2PO_4^-$  dopant ion.  $[M - H + H + D]$  illustrates the way to calculate the  $m/z$  of  $[M + D]^-$  ions.

Afterwards, all  $m/z$  values with  $R > 2$  were used for further elucidation, representing significantly defined intensity differences in the absence or presence of anionic dopants. For clarification, intensities corresponding to  $[M - H]^-$  ions from solution 00 were greater than  $1 \times 10^6$  (average noise intensity) ensuring that all used  $m/z$  ratios represent analytes and not noise signals.

## 2.7 | $m/z \rightarrow$ molecular formula calculator (in-house software)

Molecular formulas were combinatorially calculated within a mass accuracy window of  $\pm 0.2$  ppm for each peak in batch mode by an



**SCHEME 1** Workflow for the non-targeted analysis of oak plant samples [Color figure can be viewed at wileyonlinelibrary.com]

in-house software tool. The maximum number of heteroatoms allowed was C<sub>100</sub>, O<sub>80</sub>, N<sub>5</sub>, S<sub>3</sub>, Cl<sub>1</sub>/P<sub>1</sub>.

## 2.8 | Formula validation (Python)

Molecular formulas were validated via the senior-rule approach/cyclomatic number<sup>25</sup> by considering the “seven golden rules” of Kind et al.<sup>26</sup>

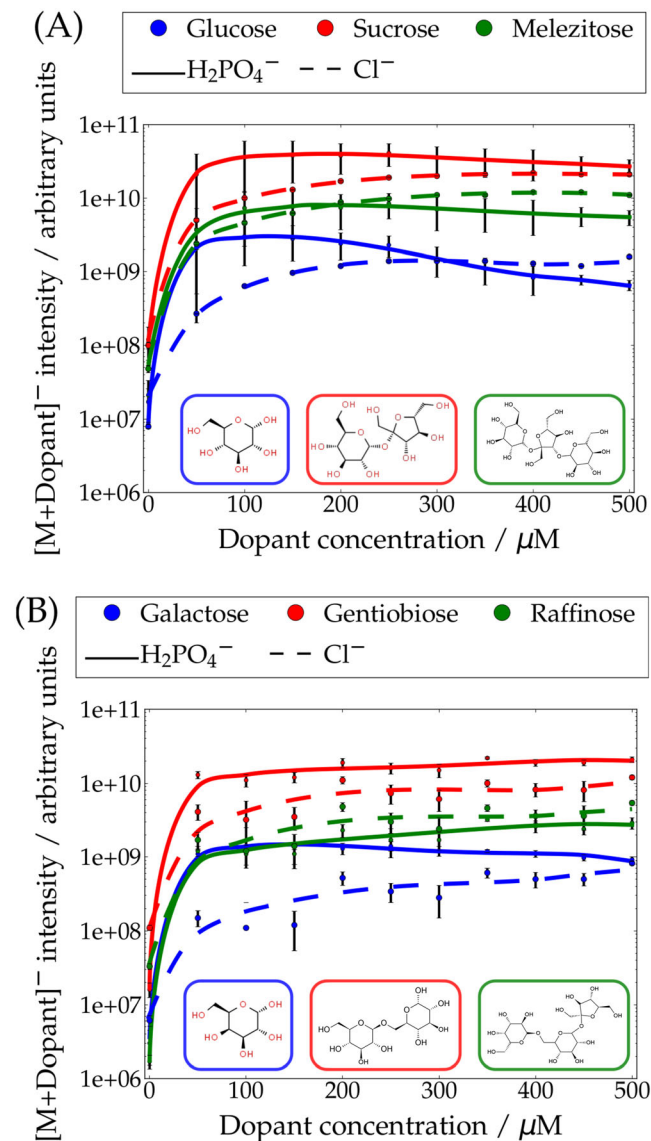


**FIGURE 1** FT-ICR-MS signal intensity profile (log Y scale) along elevated spiked dopant concentrations of NH<sub>4</sub>Cl and NH<sub>4</sub>H<sub>2</sub>PO<sub>4</sub> for A, sugar mixture of glucose ( $\alpha$  and  $\beta$  anomers), sucrose and melezitose; B, sugar mixture of galactose ( $\alpha$  and  $\beta$  anomers), gentiobiose and raffinose. For measured triplicates, mean intensity values are plotted with standard deviations and 4<sup>th</sup> order polynomial fits [Color figure can be viewed at wileyonlinelibrary.com]

## 2.9 | Data-analytical workflow for the non-targeted analysis of oak plant samples

Five solutions with different dopant concentrations were measured (dopant concentration of 0 μM, 25 μM, 50 μM, 100 μM, 200 μM → solution 00, solution 01, solution 02, solution 03, solution 04), using triplicates for each concentration, added to the plant stock solution. The data-analytical workflow for the non-targeted analysis of oak plant samples is represented in Scheme 1.

## 3 | RESULTS AND DISCUSSION

Sugars can be deprotonated in an electrospray ionization (ESI) source to produce [M – H]<sup>-</sup> ions but their MS signal intensities are very low due to high deprotonation energies.<sup>7,26</sup> Dopants represent powerful agents in ESI-MS allowing the detection of organic molecules which cannot be easily ionized.<sup>8–11</sup> NH<sub>4</sub>H<sub>2</sub>PO<sub>4</sub> as a dopant can enable an effective way for the ionization of saccharides due to attachment of the H<sub>2</sub>PO<sub>4</sub><sup>-</sup> dopant anion into the sugar molecule, giving rise to very high signal intensities, when compared to those of [M – H]<sup>-</sup> ions (Figure S1, supporting information).

Figure 1 shows MS signal intensity profiles for two sugar mixtures A: Glucose (monosaccharide), sucrose (disaccharide) and melezitose (trisaccharide) as well as B: Galactose (monosaccharide), gentiobiose (disaccharide) and raffinose (trisaccharide) as a function of the concentration of the spiked dopants. As can be experimentally discerned from Figure 1 and computationally concluded (through examining sugars affinities toward the dopant ion) from Figure 2, ion

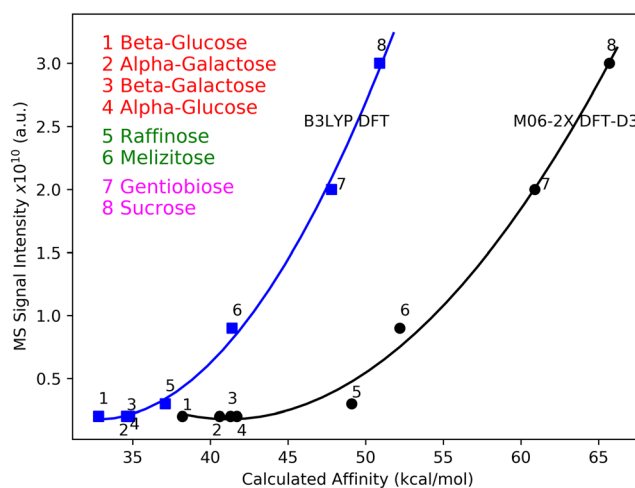


**FIGURE 2** FT-ICR-MS maximum signal intensity curves vs. calculated saccharide affinities toward the H<sub>2</sub>PO<sub>4</sub><sup>-</sup> dopant anion. Quadratic fits are shown as curves: Blue for B3LYP/6-311+(2d,p)//B3LYP/6-31+(d,p) and black for the dispersion corrected DFT-D3 M06-2X/Def2TZVP//M06-2X/Def2TZVP. Monosaccharides are shown in red; trisaccharides are shown in green; and disaccharides in cyan [Color figure can be viewed at wileyonlinelibrary.com]

production of  $[M + D]^-$  increases in the direction: Monosaccharides < Trisaccharides < Disaccharides. The main interaction is non-covalent due to formation of multiple hydrogen bonds between the several OH groups in the saccharides and the dopant anion.

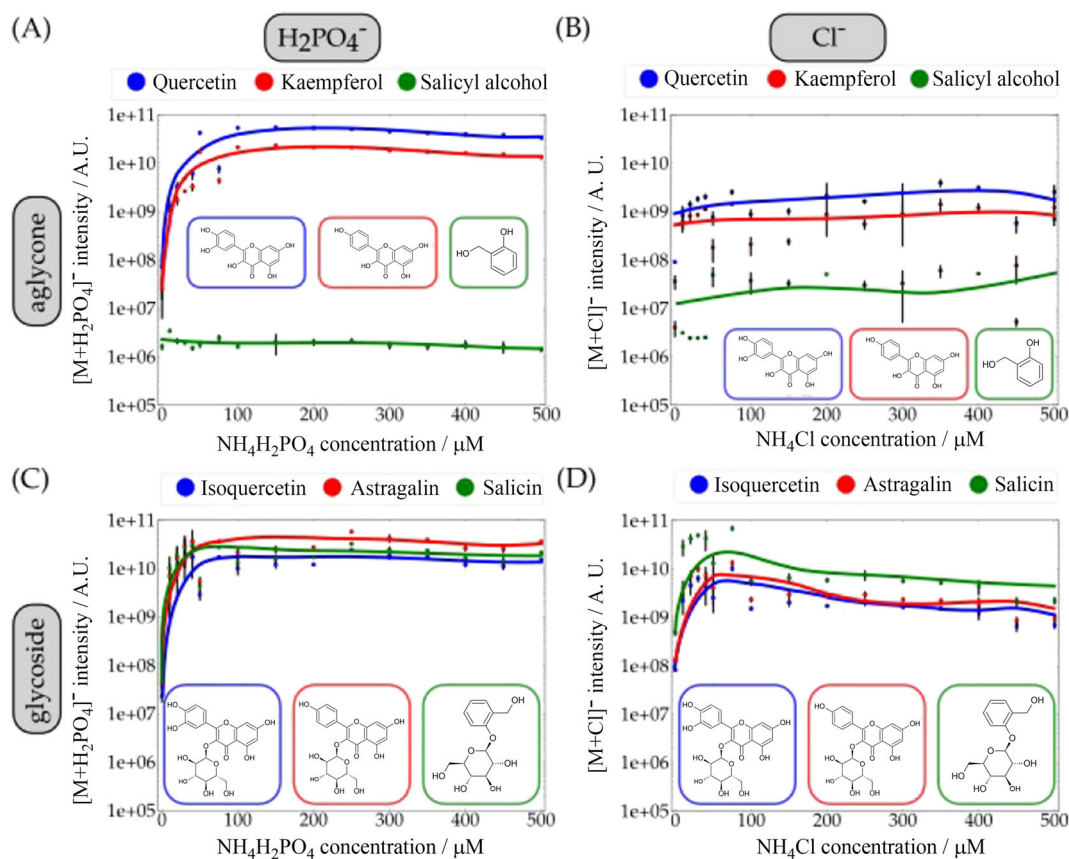
However,  $H_2PO_4^-$  gives a stronger and larger number of H-bonds, when compared with the  $Cl^-$  anion. Due to the fact that the effective ion radius (>269 pm) of the  $H_2PO_4^-$  dopant is much greater than that of a simple  $Cl^-$  ion (167 pm),<sup>27</sup> the  $H_2PO_4^-$  dopant can more effectively interact with several saccharide OH groups to form multiple H-bonds with the sugar substrate. The optimized geometries of the  $H_2PO_4^-$  adduct anions for the examined sugar mixtures are shown in Figure S2 (supporting information). Disaccharides can donate the largest number of H-bonds toward the dopant anion when compared with mono- and trisaccharides. Addition of more sugar rings to disaccharides does not increase the affinity of the trisaccharide toward  $H_2PO_4^-$  due to steric hindrance and conformational limits in the geometry. This is experimentally validated as shown in Figures 1 and S1, supporting information) in accordance with the calculated affinities shown in Figure 2.

Figure 2 shows a key correlation between the experimental steady-state maximum MS signal intensities of the formed adduct

ions and the calculated sugar affinities toward the  $H_2PO_4^-$  anion, confirming the increased order of sensitivity and affinities in the direction: Monosaccharides < Trisaccharides < Disaccharides. The dispersion corrected DFT-D3<sup>28</sup> method gives more accurate results,<sup>29</sup> showing higher variation in the obtained affinities. This correlates with higher ion production (abundance).

This new finding has a great impact on the MS detection of organic compounds in plants by glycosylation, since glycosylated organic compounds can be much better ionized for mass spectrometric investigations when compared with their aglycones. Figures 3A–3D compare experimental MS intensity profiles for  $H_2PO_4^-$  complexes towards aglycone and glycosidic dopant systems (including  $Cl^-$  systems for reference). For both dopants,  $H_2PO_4^-$  and  $Cl^-$ , similar binding has been observed for quercetin/isoquercetin and kaempferol/stragalgin whereas it was different for salicyl alcohol/salicin. The aglycones quercetin and kaempferol could be detected in both forms  $[M + H_2PO_4]^-$  and  $[M + Cl]^-$  (with M = neutral substrate) and so were their glycosidic forms, isoquercetin and astragalgin.

Thus, the  $H_2PO_4^-$  dopant anion does not necessarily require a sugar moiety to attach to but can also bind to the aglycone itself. For



**FIGURE 3** (A–D) Intensity MS profiles (log Y scale) of  $[M + \text{dopant}]^-$  anions for varying  $NH_4H_2PO_4$  (left column, A, C) or  $NH_4Cl$  (right column, B, D) in an aglycone (1st row, A, B) or glycoside mixture (2nd row, C, D), with M = aglycone/glycoside substrate. Mean values for measured triplicates are plotted with standard deviations. Curve fitting was done by 4<sup>th</sup> order polynomials [Color figure can be viewed at [wileyonlinelibrary.com](http://wileyonlinelibrary.com)]

chloride anion attachment, stronger binding has been observed toward the glycosidic part when compared with the aglyconic region (cf. isoquercetin-Cl<sup>-</sup>, astragalín-Cl<sup>-</sup>, salicin-Cl<sup>-</sup>). Salicyl alcohol could barely be detected as the [M + Cl]<sup>-</sup> complex with low intensities only (not detected as the [M + H<sub>2</sub>PO<sub>4</sub>]<sup>-</sup> complex) while its glycosylated form, salicin, gave both intense [M + H<sub>2</sub>PO<sub>4</sub>]<sup>-</sup> and [M + Cl]<sup>-</sup> signals. Due to the unique pattern of the salicyl alcohol/salicin system (as can be significantly discerned when comparing Figure 3A with 3C), we focused on performing a thorough theoretical investigation of this system when it interacts with the H<sub>2</sub>PO<sub>4</sub><sup>-</sup> anion.

Dissociation energies of the formed product ions for salicyl alcohol and salicin with H<sub>2</sub>PO<sub>4</sub><sup>-</sup> were also computed to obtain insight into the most favorite site-specific binding site toward the dopant anion (Table 1). These findings are well explained by

**TABLE 1** Dissociation energies (kcal/mol) of the [Salicyl alcohol – H<sub>2</sub>PO<sub>4</sub>]<sup>-</sup> complex anion as well as several possible geometries for H<sub>2</sub>PO<sub>4</sub><sup>-</sup> ion attachment to salicin (2-hydroxyaryl-beta-D-glucopyranoside) according to the structures shown in Figure S3 (supporting information), calculated at the B3LYP/6-311+(2d,p)//B3LYP/6-31+(d,p) level

No.	Substrate-H <sub>2</sub> PO <sub>4</sub> <sup>-</sup> complex anion	Complex dissociation energy (kcal/mol)
1	Salicyl alcohol – H <sub>2</sub> PO <sub>4</sub> <sup>-</sup>	24.7
2	Salicin – H <sub>2</sub> PO <sub>4</sub> <sup>-</sup> (attachment to aglycone)	24.3
3	Salicin – H <sub>2</sub> PO <sub>4</sub> <sup>-</sup> (formation of a pseudo-ring)	29.0
4	Salicin – H <sub>2</sub> PO <sub>4</sub> <sup>-</sup> (attachment to glucose)	34.2

examining the optimized adduct ion geometries of salicyl alcohol and salicin with H<sub>2</sub>PO<sub>4</sub><sup>-</sup> (Figure S3, supporting information). An application of the usage of H<sub>2</sub>PO<sub>4</sub><sup>-</sup> as a potential ESI-MS dopant is introduced by examining the diverse H<sub>2</sub>PO<sub>4</sub><sup>-</sup> adduct ions, formed in an oak sample (oak *Quercus robur* from North-Rhine Westphalia<sup>18</sup>) by means of a non-targeted, high-resolution FT-ICR-MS analysis. A Matlab-based program was written to specifically extract features which uniquely form either H<sub>2</sub>PO<sub>4</sub><sup>-</sup> or Cl<sup>-</sup> dopant complexes, after filtering the noise according to a home-made algorithm.<sup>24</sup>

Around 50% of the identified substrate molecules M would not have been detected as [M – H]<sup>-</sup> ions ([M – H]<sup>-</sup> intensity in the noise level). These substrate molecules M show at least an intensity onset of factor 2 in form of their dopant ions ( $|[M + \text{Dopant}]^-|/[M - H]^- \geq 2$ ). Details about the data analytical workflow is given in section 2.9 (Scheme 1).

Figure 4 illustrates that H<sub>2</sub>PO<sub>4</sub><sup>-</sup> and Cl<sup>-</sup> specifically form dopant complexes with neutral substrate molecules M. Here, a modified van Krevelen diagram demonstrates the chemical characteristics of neutral substrates M by plotting their H/C ratios vs. *m/z*, masses. Molecular formulas for neutral substrate compounds M were calculated based on the analysis of [M + H<sub>2</sub>PO<sub>4</sub>]<sup>-</sup> and [M + Cl]<sup>-</sup> ions. Compounds M may correspond to ones that are hardly ionizable, e.g. lignin precursors. While 98 *m/z* features (compounds + isomers) form specific Cl<sup>-</sup> dopant complexes were discerned, 139 unique H<sub>2</sub>PO<sub>4</sub><sup>-</sup> complexes could be detected. This finding from non-targeted analysis of a complex plant sample is in agreement with the above discussed targeted investigations, indicating that H<sub>2</sub>PO<sub>4</sub><sup>-</sup> binds stronger toward organic substrates (sugars and other organic classes) than Cl<sup>-</sup> does.

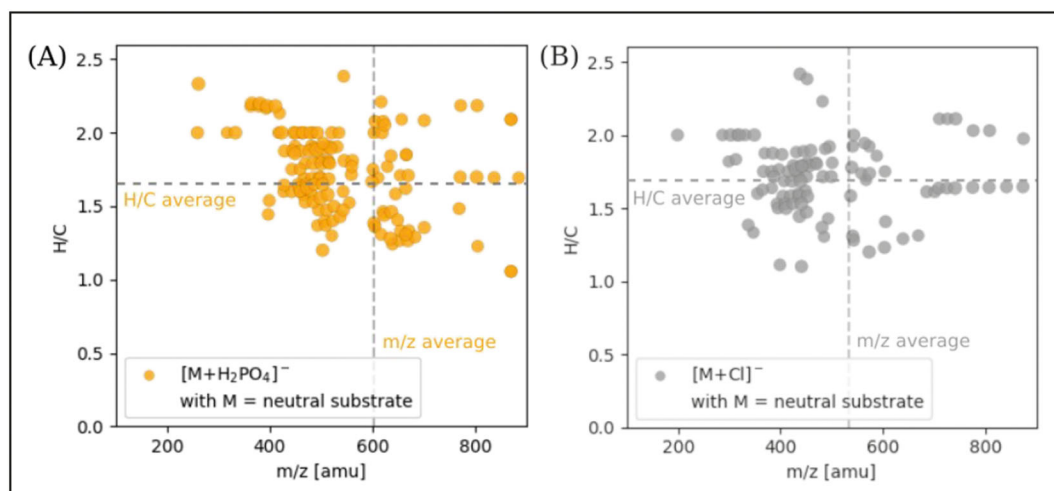


**FIGURE 4** Specific dopant complexes in a complex oak plant sample. This modified van Krevelen diagram (H/C vs. *m/z* ratio plot) highlights compounds present in the oak sample which form H<sub>2</sub>PO<sub>4</sub><sup>-</sup> (orange, A) and Cl<sup>-</sup> dopant complexes (gray, B). The bubble size is scaled by log (intensity). Dashed lines represent average values for H/C or *m/z*, respectively [Color figure can be viewed at [wileyonlinelibrary.com](http://wileyonlinelibrary.com)]

## 4 | CONCLUSIONS

$\text{H}_2\text{PO}_4^-$  enables the detection of compounds which would be challenging to detect in the absence of the  $\text{H}_2\text{PO}_4^-$  dopant. According to the previously shown correlation diagram between MS signal intensities of detected  $[\text{M} + \text{H}_2\text{PO}_4]^-$  anions of different saccharides and their calculated dissociation enthalpies, an excellent agreement with a coefficient of determination  $R^2 = 99\%$  could be achieved. Thus, the variation in MS signal intensities can be very well described to a large extent by variation in calculated saccharide affinities toward the  $\text{H}_2\text{PO}_4^-$  dopant anion, showing that the DFT-D3 method can very well describe experimental FT-ICR-MS observations. Both DFT and DFT-D3 calculations gave clear reasons for the noticeably increased ion production and calculated affinities in the order: Monosaccharides < Trisaccharides < Disaccharides. The site-specific attachment of the  $\text{H}_2\text{PO}_4^-$  dopant anion to different saccharides and to glycosylated organic compounds could be revealed, explaining the role of glycosylation for enhancing the ionization efficiency of the detected organic compounds, when the  $\text{H}_2\text{PO}_4^-$  anion is used as a dopant in ESI-MS experiments.

## ACKNOWLEDGEMENTS

The authors would like to thank Dr. Andrea Ghirardo and Moritz Kaling (Helmholtz Zentrum München) for providing the plant samples.

## DATA AVAILABILITY STATEMENT

Data available on request from the authors

## ORCID

Basem Kanawati  <https://orcid.org/0000-0003-3391-5365>

## REFERENCES

- Ruiz-Mirazo K, Briones C, de la Escosura A. Prebiotic systems chemistry: New perspectives for the origins of life. *Chem Rev*. 2014; 114(1):285-366. doi:10.1021/cr2004844
- Dworkin JP, Lazcano A, Miller SL. The roads to and from the RNA world. *J Theor Biol*. 2003;222(1):127-134. doi:10.1016/S0022-5193(03)00020-1
- Meinert C, Myrgorodska I, De Marcellus P, et al. Ribose and related sugars from ultraviolet irradiation of interstellar ice analogs. *Science*. 2016;352(6282):208-212. doi:10.1126/science.aad8137
- Levy DE, Fügedi P. *The Organic Chemistry of Sugars*. Boca Raton: CRC Press; 2005. doi:10.1201/9781420027952
- Wan ECH, Yu JZ. Analysis of sugars and sugar polyols in atmospheric aerosols by chloride attachment in liquid chromatography/negative ion electrospray mass spectrometry. *Environ Sci Technol*. 2007;41(7):2459-2466. doi:10.1021/es062390g
- Jiang Y, Cole RB. Oligosaccharide analysis using anion attachment in negative mode electrospray mass spectrometry. *J Am Soc Mass Spectrom*. 2005;16(1):60-70. doi:10.1016/j.jasms.2004.09.006
- Boutegrabet L, Kanawati B, Gebefügi I, et al. Attachment of chloride anion to sugars: Mechanistic investigation and discovery of a new dopant for efficient sugar ionization/detection in mass spectrometers. *Chem a Eur J*. 2012;18(41):13059-13067. doi:10.1002/chem.201103788
- Khairallah G, Peel JB. Cyano adduct anions of C70: Electrospray mass spectrometric studies. *J Phys Chem A*. 1997;101(36):6770-6774. doi:10.1021/jp970635t
- Cole RB, Zhu J. Chloride anion attachment in negative ion electrospray ionization mass spectrometry. *Rapid Commun Mass Spectrom*. 1999;13(7):607-611. doi:10.1002/(SICI)1097-0231(19990415)13:7<3C607::AID-RCM530%3E3.0.CO;2-2
- Bayer E, Gfrörer P, Rentel C. Coordination-ionspray-MS (CIS-MS), a universal detection and characterization method for direct coupling with separation techniques. *Angew Chem Int Ed*. 1999;38(7):992-995. doi:10.1002/(SICI)1521-3773(19990401)38:7<3C992::AID-ANIE992%3E3.0.CO;2-K
- Cai Y, Concha MC, Murray JS, Cole RB. Evaluation of the role of multiple hydrogen bonding in offering stability to negative ion adducts in electrospray mass spectrometry. *J Am Soc Mass Spectrom*. 2002;13(12):1360-1369. doi:10.1016/S1044-0305(02)00648-7
- Cerda BA, Wesdemiotis C. The relative copper(I) ion affinities of amino acids in the gas phase. *J Am Chem Soc*. 1995;117(38):9734-9739. doi:10.1021/ja00143a017
- Cerda BA, Wesdemiotis C. Thermochemistry and structures of Na+ coordinated mono- and disaccharide stereoisomers. *Int J Mass Spectrom*. 1999;189(2-3):189-204. doi:10.1016/S1387-3806(99)00085-8
- Tian Y, Chen W, Zhao Z, Xu L, Tong B. Interaction and selectivity of 14-crown-4 derivatives with  $\text{Li}^+$ ,  $\text{Na}^+$  and  $\text{Mg}^{2+}$  metal ions *J Mol Model*. 2020;26(4):67-79. doi:10.1007/s00894-020-4325-8
- Harvey DJ. Negative ion mass spectrometry for the analysis of n-linked glycans. *Mass Spectrom Rev*. 2020;39(5-6):586-679. doi:10.1002/mas.21622
- Nimtz M, Wray V, Rüdiger A, Conradt HS. Identification and structural characterization of a mannose-6-phosphate containing oligomannosidic N-glycan from human erythropoietin secreted by recombinant BHK-21 cells. *FEBS Lett*. 1995;365(2-3):203-208. doi:10.1016/0014-5793(95)00473-M
- Blanchard V, Gadkari RA, Gerwig GJ, Leeflang BR, Dighe RR, Kamerling JP. Characterization of the N-linked oligosaccharides from human chorionic gonadotropin expressed in the methylotrophic yeast *Pichia pastoris*. *Glycoconjugate J*. 2007;24(1):33-47.
- Ghirardo A, Heller W, Fladung M, Schnitzler JP, Schroeder H. Function of defensive volatiles in pedunculate oak (*Quercus robur*) is tricked by the moth *Tortrix viridana*. *Plant Cell Environ*. 2012;35(12):2192-2207. doi:10.1111/j.1365-3040.2012.02545.x
- Frisch MJ, Trucks GW, Schlegel HB, et al. *Gaussian 09, Revision D.01*. Wallingford, CT: Gaussian, Inc.; 2016.
- Schlegel HB. Optimization of equilibrium geometries and transition structures *J Comput Chem*. 1982;3(2):214-218. doi:10.1002/jcc.540030212
- Schlegel HB. Estimating the hessian for gradient-type geometry optimizations. *Theor Chim Acta*. 1984;66(5):333-340. doi:10.1007/BF00554788
- Dennington R, Keith T, Millam J, Eppinnett K, Hovell WL, Gilliland R, GaussView, 2003.
- Foreman JB, Frisch A. *Exploring Chemistry with Electronic Structure Methods*. 2nd ed. Pittsburgh: Gaussian, Inc.; 1993.
- Kanawati B, Bader TM, Wanczek KP, Li Y; Schmitt-Kopplin P. Fourier transform (FT)-artifacts and power-function resolution filter in Fourier transform mass spectrometry. *Rapid Commun Mass Spectrom*. 2017;31(19):1607-1615. doi:10.1002/rcm.7940
- Senior JK. Partitions and their representative graphs. *Am J Math*. 1951;73(3):663. doi:10.2307/2372318
- Kind T, Fiehn O. Seven Golden rules for heuristic filtering of molecular formulas obtained by accurate mass spectrometry. *BMC Bioinformatics*. 2007;8(1):105. doi:10.1186/1471-2105-8-105
- Shannon RD. Revised effective ionic radii and systematic studies of interatomic distances in halides and chalcogenides. *Acta Crystallogr A*. 1976;32(5):751-767. doi:10.1107/S0567739476001551

28. Grimme S, Antony J, Ehrlich S, Krieg H. A consistent and accurate ab initio parametrization of density functional dispersion correction (DFT-D) for the 94 elements H-Pu. *J Chem Phys.* 2010;132(154104): 1-19. doi:10.1063/1.3382344
29. Hujo W, Grimme S. Comparison of the performance of dispersion-corrected density functional theory for weak hydrogen bonds. *Phys Chem Chem Phys.* 2011;13(31):13942-13950. doi:10.1039/c1cp20591a

**How to cite this article:** Ruf A, Kanawati B, Schmitt-Kopplin P. Dihydrogen phosphate anion boosts the detection of sugars in electrospray ionization mass spectrometry: A combined experimental and computational investigation. *Rapid Commun Mass Spectrom.* 2022;36(11):e9283. doi:10.1002/rcm.9283

## SUPPORTING INFORMATION

Additional supporting information may be found in the online version of the article at the publisher's website.